Stem Cell Reports, Volume *8*

Supplemental Information

Dysregulation of the SIRT1/OCT6 Axis Contributes to Environmental Stress-Induced Neural Induction Defects

Guoping Li, Zeyidan Jiapaer, Rong Weng, Yi Hui, Wenwen Jia, Jiajie Xi, Guiying Wang, Songcheng Zhu, Xin Zhang, Dandan Feng, Ling Liu, Xiaoqing Zhang, and Jiuhong Kang

SUPPLEMENTAL FIGURES

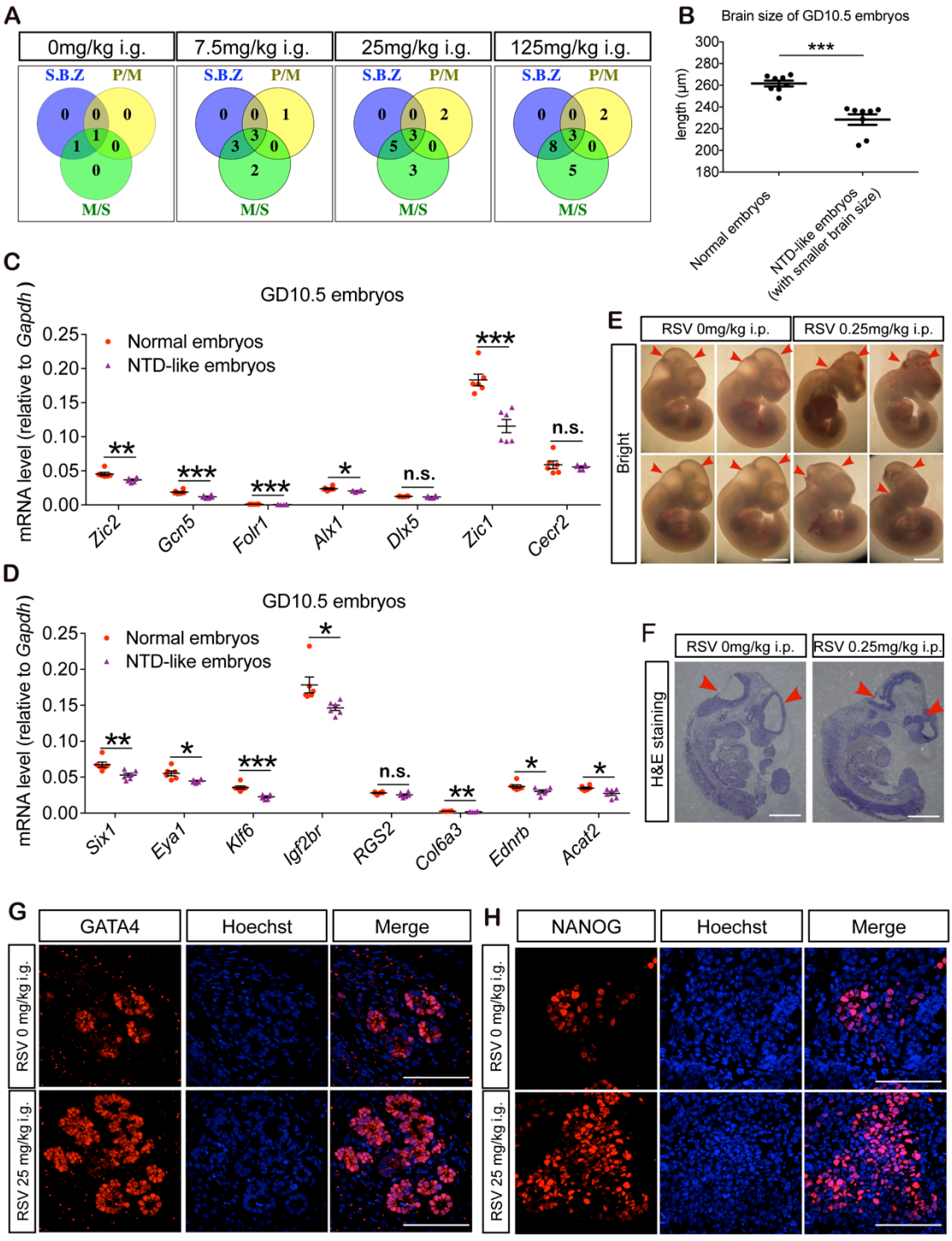

Figure S1. RSV Induces NTD-like Phenotypes *In Vivo*, Related to Figure 1.

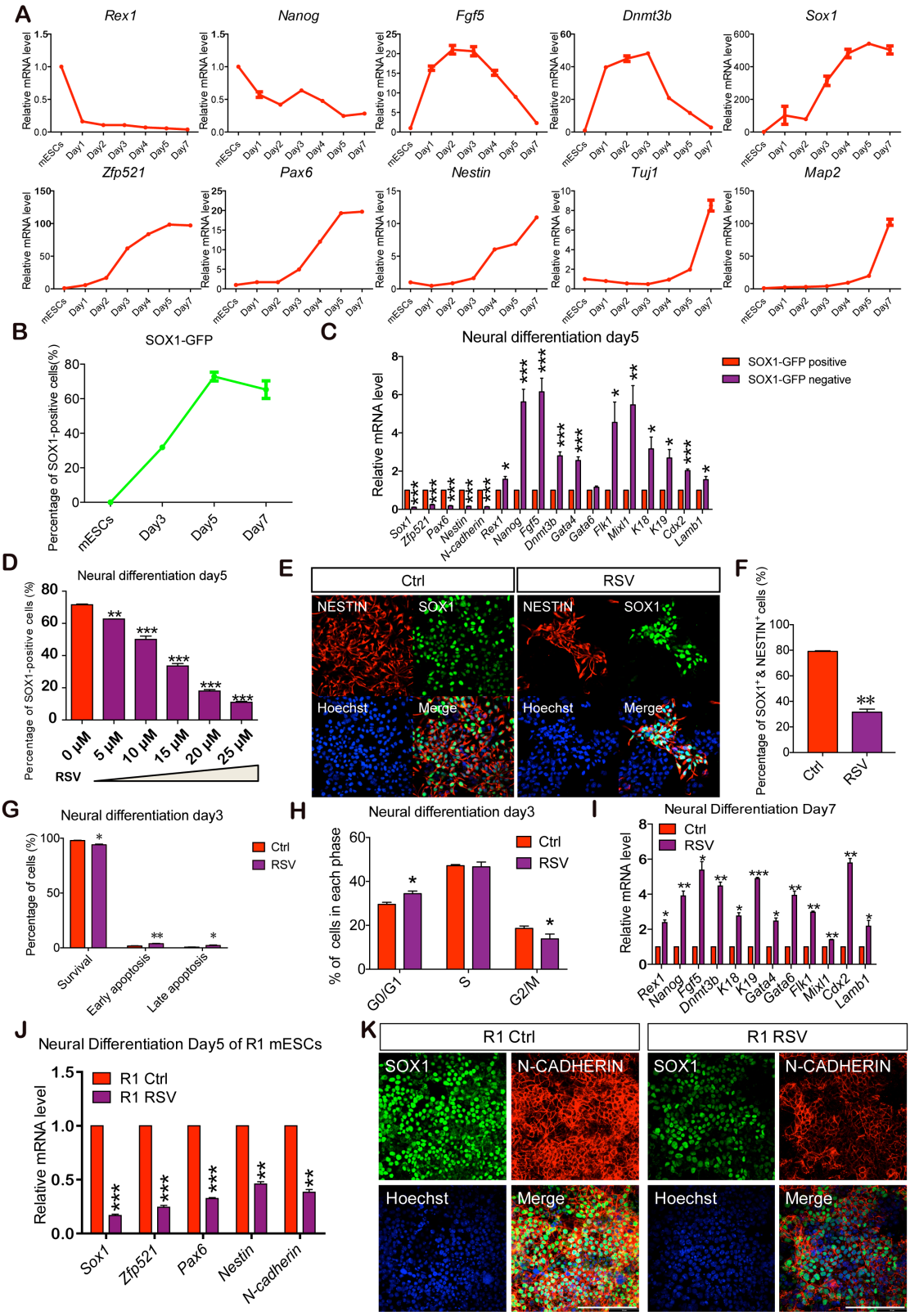

Figure S2. RSV Hinders the Neural Differentiation of mESCs *In Vitro*, Related to Figure 2.

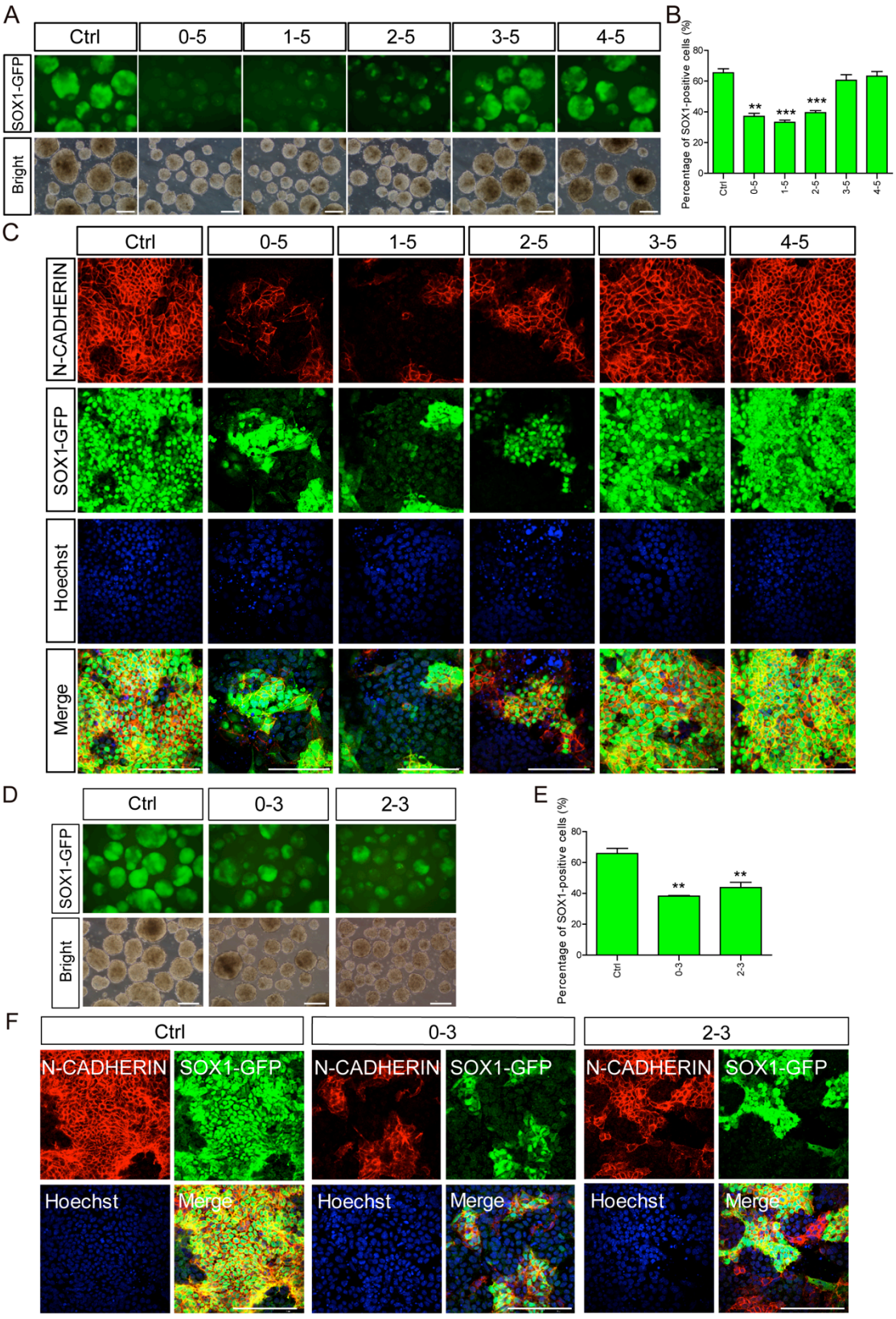

Figure S3. RSV Specifically Hinders the Neural Induction Process During Neural Differentiation, Related to Figure 2.

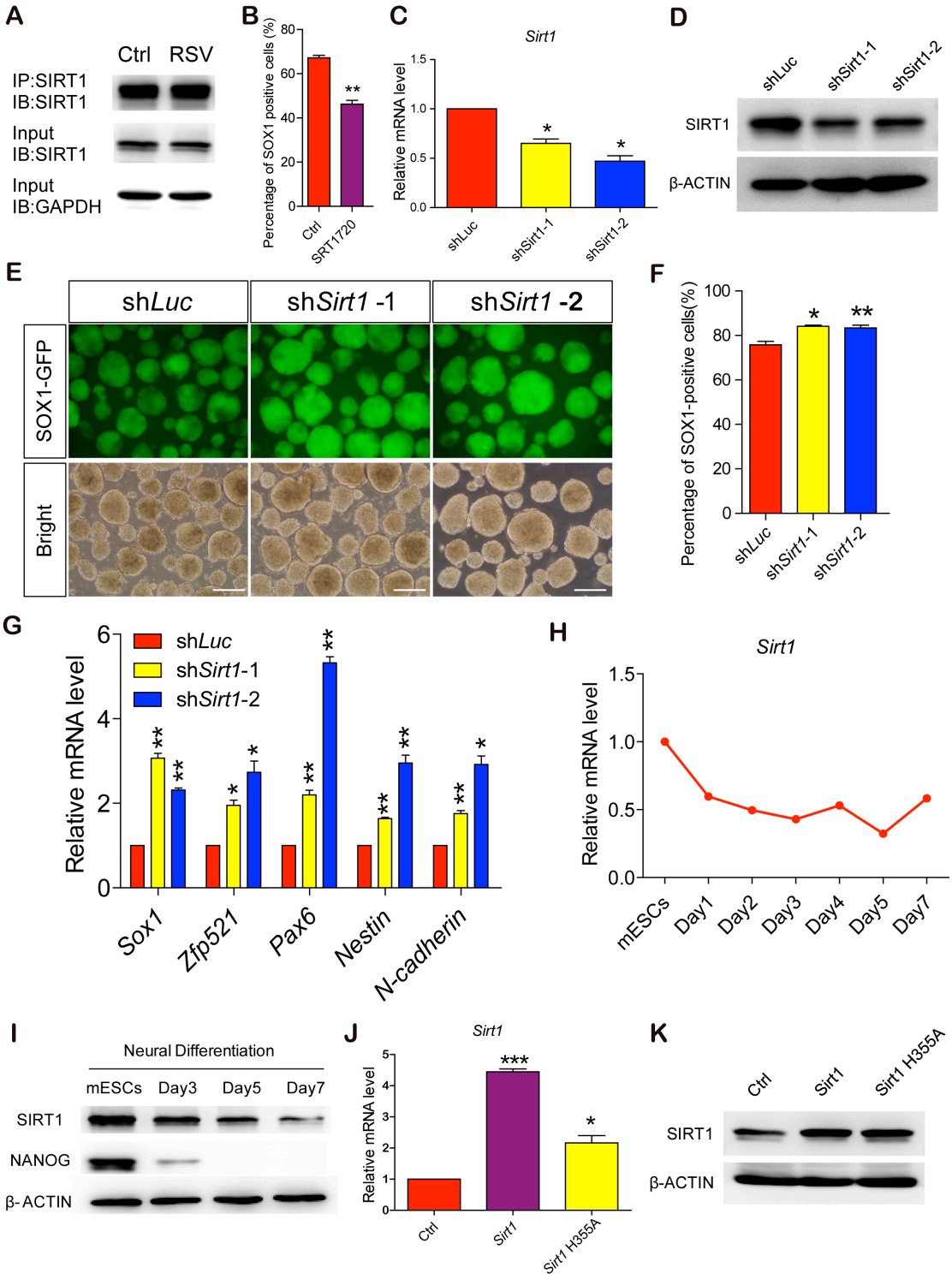

Figure S4. Targeting *Sirt1* in mESCs and the Negative Correlation Between *Sirt1* Expression and Neural Induction Efficiency, Related to Figure 3.

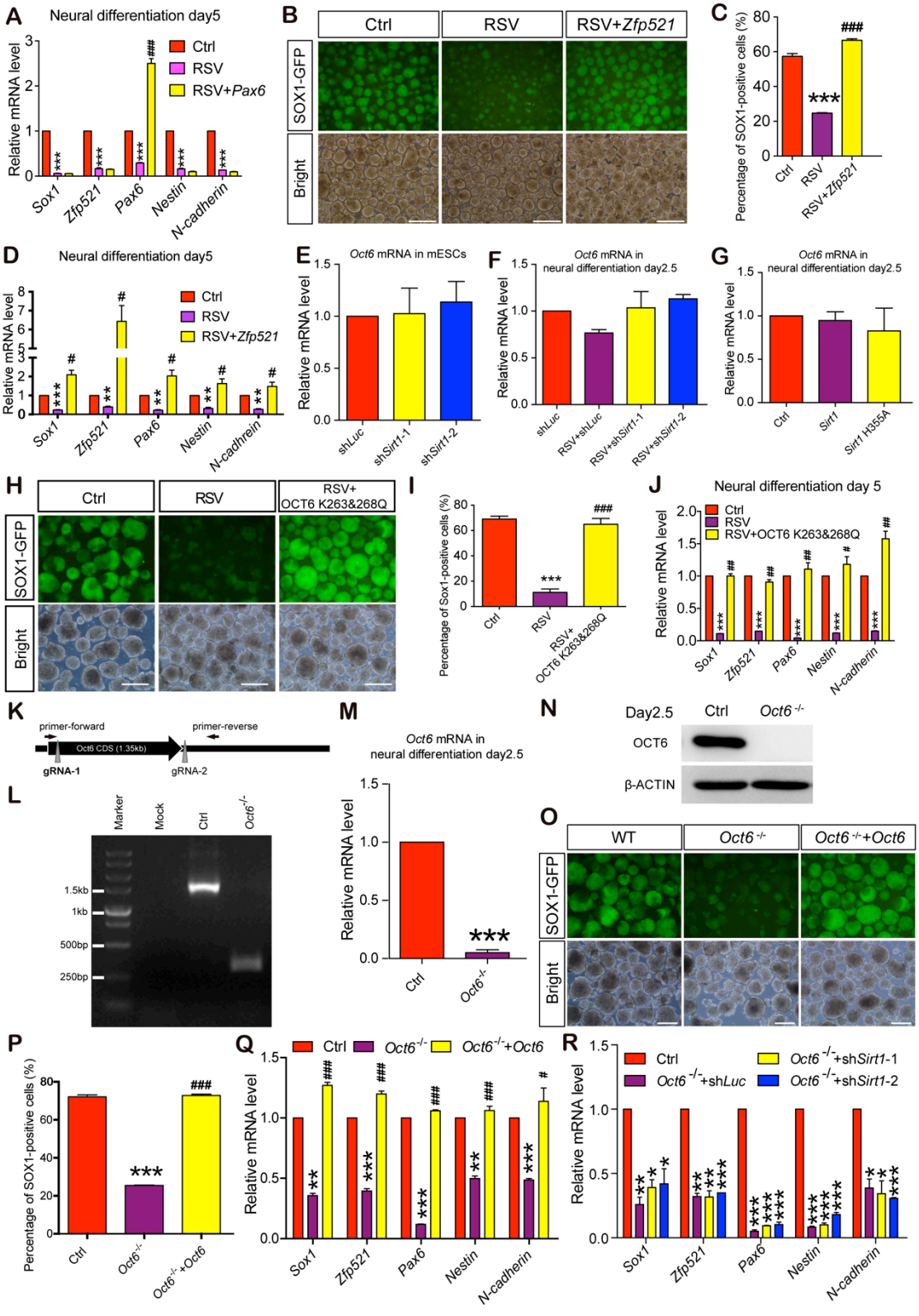

Figure S5. The *Oct6/Zfp521* Pathway is Truly Responsible for the Neural Induction Defects Triggered by RSV Treatment, Related to Figure 4.

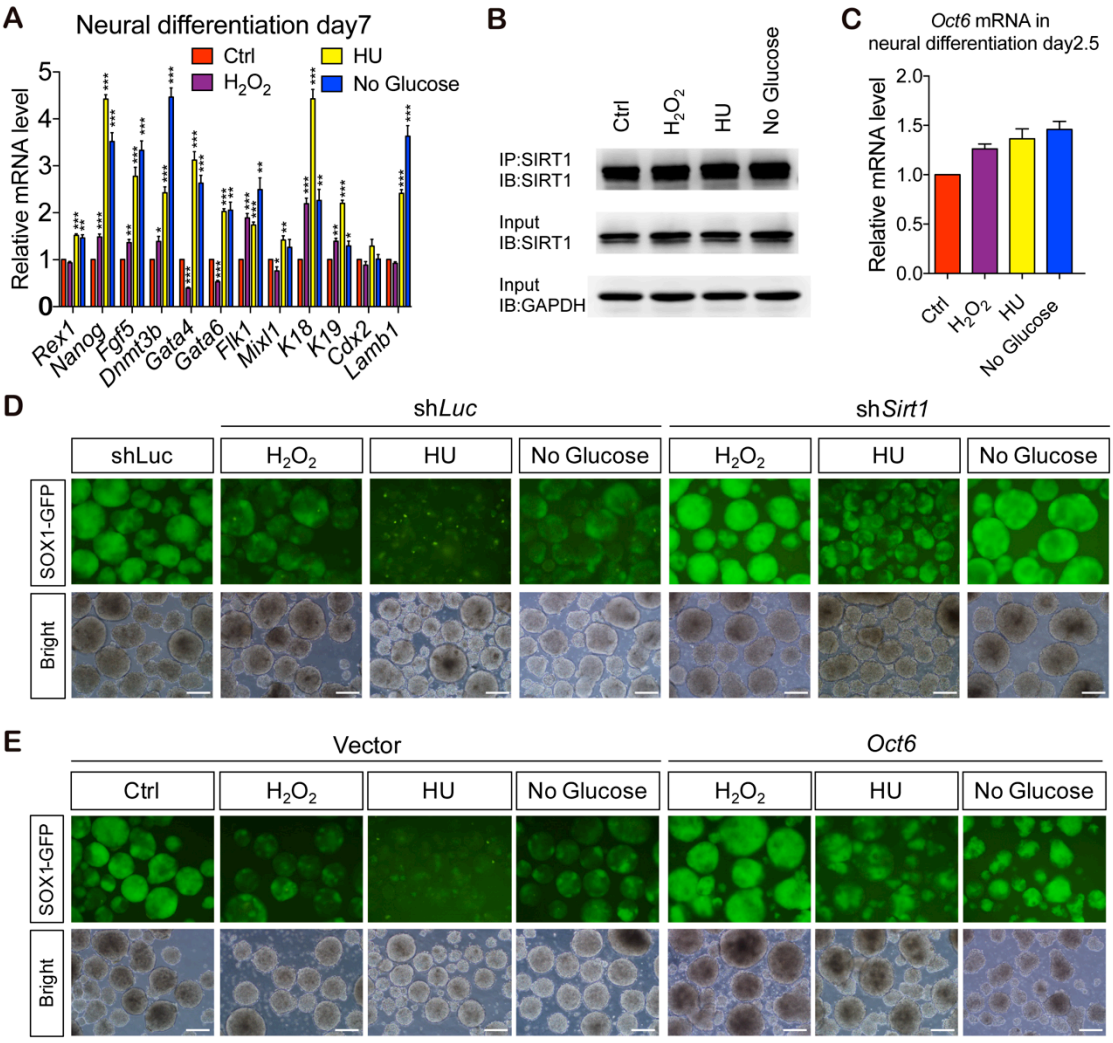

Figure S6. The SIRT1/OCT6 Axis is Required for the Induction of Neural Induction Defects by Environmental Stresses, Related to Figure 5.

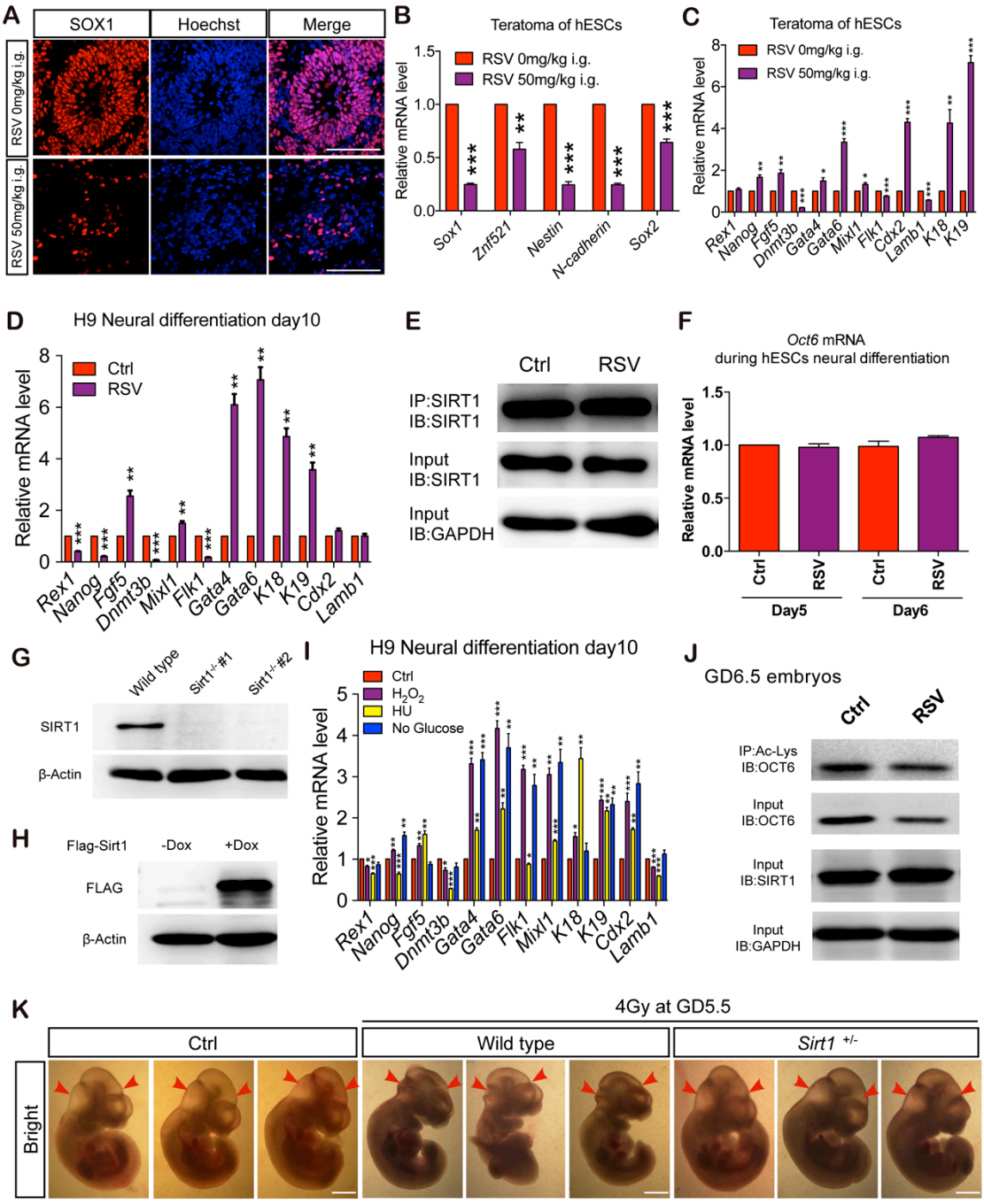

Figure S7. The Functional Role of the SIRT1/OCT6 Axis is Conserved in Humans and is Recapitulated in Radiation-induced NTDs, Related to Figure 6 and 7.

SUPPLEMENTAL FIGURE LEGENDS

Figure S1. RSV Induces NTD-like Phenotypes *In Vivo*, Related to Figure 1.

(A) The number of embryos exhibiting each neurological malformation, including smaller brain size (S.B.Z.), increased indentations between the prosencephalon/metencephalon (P/M) or metencephalon/spinal cord (M/S), after maternal different dosages of RSV administration.
(B) The brain sizes (length from prosencephalon to metencephalon) of normal embryos and RSV-induced NTD-like embryos that exhibit a smaller brain size.
(C and D) The expression level of NTD-risk genes in GD10.5 normal embryos and RSV-induced NTD-like embryos.
(E) Maternal intraperitoneal (i.p.) RSV delivery from GD3.5 to GD10.5 similarly induces NTD-like phenotypes in embryos at GD10.5. Red arrowheads indicate the prosencephalon/metencephalon and metencephalon/spinal cord junctions.
(F) Representative H&E staining of embryos in (E).
(G and H) Immunostaining of GATA4 (G) and NANOG (H) in mouse teratomas with or without RSV administration.
Data are shown as the means ± SEM of at least three independent experiments. Unpaired two-tailed Student's *t*-test. n.s. $p>0.05$, * $p<0.05$, ** $p<0.01$, *** $p<0.001$ versus the control. Scale bar, 100 μm.

Figure S2. RSV Hinders the Neural Differentiation of mESCs *In Vitro*, Related to Figure 2.

(A) Sequential downregulation and activation of pluripotent genes, epiblast genes, neuroepithelial genes and neuronal genes during the neural differentiation of 46C mESCs.
(B) FACS analysis showing the increased expression of the GFP reporter construct during the neural differentiation of 46C mESCs.
(C) Expression level of germ-layer genes in SOX1-GFP-negative or positive cells.
(D) RSV hinders the neural differentiation of 46C mESCs in a dose-dependent manner.
(E) RSV significantly suppresses the formation of neural stem cells, which were labeled by SOX1 and NESTIN.
(F) Formation rate of neural stem cells in (E).
(G and H) RSV treatment slightly affects the apoptosis (G) or cell cycle (H) of differentiated mESCs.
(I) RSV treatment elevates the expression of non-neural-lineage genes.
(J and K) RSV treatment (30 μM) similarly hinders the neural differentiation of R1 mESCs, as shown by Q-PCR (J) and immunostaining (K) analysis in day 5 SFEBs.
Data are shown as the means ± SEM of three independent experiments. Unpaired two-tailed Student's *t*-test. * $p<0.05$, ** $p<0.01$, *** $p<0.001$ versus the control. Scale bar, 100 μm.

Figure S3. RSV Specifically Hinders the Neural Induction Process During Neural Differentiation, Related to Figure 2.

(A-C) RSV was applied to differentiated mESCs at the indicated time points until day 5, and the most significant suppression of neural differentiation was achieved when RSV was added at day 0, 1 and 2, as shown by microscopy (A), FACS (B), and immunostaining (C) analysis in day 5 SFEBs.
(D-F) RSV treatment, from days 0 to 3 or days 2 to 3, is sufficient to inhibit neural differentiation, as shown by microscopy (D), FACS (E), and immunostaining (F) analysis in day 5 SFEBs.
Data are shown as the means ± SEM of three independent experiments. Unpaired two-tailed Student's *t*-test. ** $p<0.01$, *** $p<0.001$ versus the control. Scale bar, 100 μm.

Figure S4. Targeting *Sirt1* in mESCs and the Negative Correlation Between *Sirt1* Expression and Neural Induction Efficiency, Related to Figure 3.

(A) RSV treatment has no obvious effects on SIRT1 protein levels in day 2.5 SFEBs.
(B) FACS analysis showing that the generation of SOX1-GFP-positive neural-lineage cells is inhibited by SRT1720 treatment.
(C and D) *Sirt1* knockdown efficiency, as verified by Q-PCR (C) and western blotting (D).
(E-G) Knocking down *Sirt1* potentiates the neural differentiation of mESCs, as shown by microscopy (E), FACS (F) and Q-PCR (G) analysis in day 5 SFEBs.
(H and I) *Sirt1* mRNA (H) and protein (I) levels are gradually downregulated during neural differentiation.

(J and K) *Sirt1* and *Sirt1* H355A overexpression efficiency, as verified by Q-PCR (J) and western blotting (K).
Data are shown as the means ± SEM of three independent experiments. Unpaired two-tailed Student's *t*-test. * $p<0.05$, ** $p<0.01$, *** $p<0.001$ versus the control. Scale bar, 100 μm.

Figure S5. The *Oct6*/*Zfp521* Pathway is Truly Responsible for the Neural Induction Defects Triggered by RSV Treatment, Related to Figure 4.

(A) Overexpression of *Pax6* during neural differentiation using an inducible system, shows no effects on the results of RSV treatment, as shown by Q-PCR analysis.
(B-D) Overexpression of *Zfp521* completely rescues the neural induction defects triggered by RSV treatment, as shown by microscopy (A), FACS (B), and QPCR (C) analysis in day 5 SFEBs
(E-G) *Oct6* mRNA is marginally regulated by *Sirt1* knockdown (E and F) or overexpression (G).
(H-J) Overexpression of the OCT6 K263&268Q mutant completely rescues the neural induction defects triggered by RSV treatment, as shown by microscopy (H), FACS (I), and QPCR (J) analysis in day 5 SFEBs.
(K) Schematic representation of strategies for *Oct6* knockout in mESCs. Double gRNAs were designed to delete the *Oct6* open reading frame.
(L-N) Verification of *Oct6* knockout efficiency in mESCs via genomic DNA PCR (L), Q-PCR (M) and western blotting (N).
(O-Q) *Oct6*$^{-/-}$ mESCs fail to differentiate into neuroectodermal cells, whereas reintroducing *Oct6* rescues the efficiency of neural induction, as demonstrated by microscopy (O), FACS (P) and Q-PCR (Q) analysis in neural differentiation derivatives from mESCs on day 5.
(R) Q-PCR analysis showing that *Sirt1* knockdown fails to ameliorate the neural differentiation defects of *Oct6*$^{-/-}$ mESCs.
Data are shown as the means ± SEM of three independent experiments. Unpaired two-tailed Student's *t*-test. * $p<0.05$, ** $p<0.01$, *** $p<0.001$ versus the control. # $p<0.05$, ### $p<0.001$ versus the RSV-treated group (A, C, D, I and J) or the *Oct6* knockout group (Q and R). Scale bar, 100 μm.

Figure S6. The SIRT1/OCT6 Axis is Required for the Induction of Neural Induction Defects by Other Environmental Stresses, Related to Figure 5.

(A) H_2O_2, HU and glucose starvation elevate the expression of pluripotent and non-neural-lineage genes.
(B) H_2O_2, HU and glucose starvation show no obvious effects on SIRT1 protein levels during the neural induction stage.
(C) H_2O_2, HU and glucose starvation show no obvious effects on *Oct6* mRNA levels.
(D) Microscopy showing that *Sirt1* knockdown ameliorates the neural induction defects triggered by environmental stressors.
(E) Microscopy showing that ectopic *Oct6* expression rescues the neural induction defects triggered by environmental stress stimulation.
Data are shown as the means ± SEM of three independent experiments. Unpaired two-tailed Student's *t*-test. * $p<0.05$, ** $p<0.01$, *** $p<0.001$ versus the untreated control. Scale bar, 100 μm.

Figure S7. The Functional Role of the SIRT1/OCT6 Axis is Conserved in Humans and is Recapitulated in Radiation-Induced NTDs, Related to Figure 6 and 7.

(A) Immunostaining of SOX1 in the teratomas of hESCs with or without RSV treatment.
(B and C) Expression levels of neural-lineage (B) and non-neural-lineage genes (C) in the teratomas of hESCs with or without RSV treatment.
(D) RSV treatment elevates the expression of other germ layer genes during the neural differentiation of hESCs.
(E) RSV treatment shows no obvious effects on SIRT1 protein levels in neural-differentiation derivatives from hESCs on day 5.
(F) RSV treatment shows a marginal influence on *Oct6* mRNA levels during the neural differentiation of hESCs.
(G) Western blotting verified the efficiency of *Sirt1* knockout in hESCs.
(H) Western blotting verified the efficiency of *Sirt1* overexpression with the inducible system.
(I) H_2O_2, HU and glucose starvation elevate the expression of other germ-layer genes during the neural differentiation of hESCs.
(J) The acetylation of OCT6 in GD6.5 embryos with or without RSV treatment.

(K) Application of 4 Gy radiation at GD5.5 efficiently induces NTDs in wild-type but not Sirt1$^{+/-}$ embryos.
Data are shown as the means ± SEM of three independent experiments. Unpaired two-tailed Student's *t*-test. * $p<0.05$, ** $p<0.01$, *** $p<0.001$ versus the control. Scale bar, 100 μm.

SUPPLEMENTAL TABLE

Table S1. Primers list, related to EXPERIMENTAL PROCEDURES section

Application	Species	Gene	Forward primer	Reverse primer
QPCR	Mouse	*Gapdh*	ATGACATCAAGAAGGTGGTG	CATACCAGGAAATGAGCTTG
QPCR	Mouse	*Sirt1*	AGAACCACCAAAGCGGAAA	TCCCACAGGAGACAGAAACC
QPCR	Mouse & Human	*Sox1*	GTTTTTTGTAGTTGTTACCGC	GCATTTACAAGAAATAATAC
QPCR	Mouse	*Zfp521*	GAGCGAAGAGGAGTTTTTGG	AGTTCCAAGGTGGAGGTCAC
QPCR	Mouse & Human	*Pax6*	TCTTTGCTTGGGAAATCCG	CTGCCCGTTCAACATCCTTAG
QPCR	Mouse	*Nestin*	GAATGTAGAGGCAGAGAAAACT	TCTTCAAATCTTAGTGGCTCC
QPCR	Mouse & Human	*N-cadherin*	TCCTGATATATGCCCAAGACAA	TGACCCAGTCTCTCTTCTGC
QPCR	Mouse	*Oct6*	AGTTCGCCAAGCAGTTCAAG	TGGTCTGCGAGAACACGTTA
QPCR	Mouse	*Rex1*	GGAAGAAATGCTGAAGGTGGAGAC	AGTCCCCATCCCCTTCAATAGC
QPCR	Mouse & Human	*Nanog*	ATTCTTCCACCAGTCCCAAA	ATCTGCTGGAGGCTGAGGTA
QPCR	Mouse	*Fgf5*	AAAGTCAATGGCTCCCACGAA	GGCACTTGCATGGAGTTTTCC
QPCR	Mouse	*Dnmt3b*	CTCGCAAGGTGTGGGCTTTTGTAAC	CTGGGCATCTGTCATCTTTGCACC
QPCR	Mouse	*K18*	ATGCGCCAGTCTGTGGAG	CCTGAGATTTGGGGGCATC
QPCR	Mouse	*K19*	GGGGGTTCAGTACGCATTGG	GAGGACGAGGTCACGAAGC
QPCR	Mouse	*Gata4*	CCTGGAAGACACCCCAATCTC	AGGTAGTGTCCCGTCCCATCT
QPCR	Mouse	*Gata6*	AATGAATGGACTCAGCCGACC	CCGAGGCACCCCGTGTAA
QPCR	Mouse	*Mixl1*	ACTTTCCAGCTCTTTCAAGAGCC	ATTGTGTACTCCCCAACTTTCCC

QPCR	Mouse	*Flk1*	TTTGGCAAATACAACCCTTCAGA	GCAGAAGATACTGTCACCACC
QPCR	Mouse	*Cdx2*	CCTGCGACAAGGGCTTGTTTAG	TCCCGACTTCCCTTCACCATAC
QPCR	Mouse	*Lamb1*	CCCCAATCTCTGTGAACCATG	GCAATTTGCACCGACACTGA
QPCR	Mouse	*Klf4*	GTGCAGCTTGCAGCAGTAAC	AGCGAGTTGGAAAGGATAAAGTC
QPCR	Mouse	*Oct4*	ACATGAAAGCCCTGCAGAAGGAGCT	GAGAACGCCCAGGGTGAGCC
QPCR	Mouse	*Tuj1*	TAGACCCCAGCGGCAACTAT	GTTCCAGGTTCCAAGTCCACC
QPCR	Mouse & Human	*Map2*	GGTCACAGGGCACCTATTCA	TGTTCACCTTTCAGGACTGC
QPCR	Human	*β-Actin*	GACCTGTACGCCAACACAG	CTCAGGAGGAGCAATGATC
QPCR	Human	*Znf521*	TTCCGAGCAAGTGCAGAAAG	AAGGTTCGAGAGCACACGTTG
QPCR	Human	*Oct6*	GCTCGAGAGCCACTTTCTCA	CCAGGCGCGTATACATCGT
QPCR	Human	*Nestin*	GCCCTGACCACTCCAGTTTA	GGAGTCCTGGATTTCCTTCC
QPCR	Human	*Sox2*	GCCCTGCAGTACAACTCCAT	TGGAGTGGGAGGAAGAGGTA
ChIP-PCR	Mouse	*Zfp521*-E1	GGCATCGATGGAGAAAAAG	CATGCAATGGTATGCTAAAG
ChIP-PCR	Mouse	*Zfp521*-E2	TCATCTGAGGAAAGAGGGAGC	TTGATGGTTGCTGGGAATTG
ChIP-PCR	Mouse	*Zfp521*-E3	AGCCGTTTTGTTTCAATCACG	GGGGGAATCTTTTTGTGAAGC
ChIP-PCR	Mouse	*Pax6*	CTAGATGAGCAGTGAGGGC	CAGCTGCTCTGATTAAGATG

SUPPLEMENTAL EXPERIMENTAL PROCEDURES

Animal Studies

All procedures involving animals were approved by the Laboratory Animal Care Committee of Tongji University under the Guide for the Care and Use of Laboratory Animals (NIH Guide). All mice were maintained in a pathogen-free environment throughout the experiments, and all efforts were made to minimizing the number of animals used and their suffering.

RSV (0 mg/kg/day, 7.5 mg/kg/day, 25 mg/kg/day and 125 mg/kg/day) was intragastrically administered to pregnant mice (6~8 weeks old; male and female ICR or C57BL6 mice were obtained from the National Resource Center of Mutant Mice Model Animal Research Center (NARC), Nanjing

University (NJU), and mated randomly) between GD3.5 and GD10.5. For each RSV dosage, two pregnant mice were randomly chosen for each one of the three independent experiments. Embryos at gestational day 10.5 were then harvested and fixed with 4% formaldehyde solution for 4~8 h at 4°C, followed by dehydration with a sucrose gradient before being submitted to frozen sectioning. To verify the effect of RSV on embryonic neural tube development, RSV was also intraperitoneally injected daily from GD3.5 to GD10.5 at a dosage of 0.25 mg/kg/day.

Teratoma formation analysis of mESCs was performed by subcutaneous injection of $(10\pm2)\times10^5$ mESCs into male NOD-SCID mice (4~6 weeks old; obtained from NARC, NJU). After injection, mice were randomly and blindingly divided into two groups (three mice for each group) and were intragastrically administered 25 mg/kg/day of RSV or an equal amount of water daily. Teratomas were harvested when the size exceeded 2.0 cm in diameter and were fixed in 4% paraformaldehyde for 8~12 h before being submitted to paraffin embedding and sectioning. For the teratoma formation analysis of hESCs, hESCs clusters (300~500 clusters/100 μl) were subcutaneously injected into male NOD-SCID mice. The mice were intragastrically administered 50 mg/kg/day of RSV or an equal amount of water daily for 8 weeks.

Gene Knockdown, Knockout or Overexpression in ESCs

For *Sirt1* knockdown, two shRNAs targeting the CDS of *Sirt1* mRNA were designed (sh*Sirt1*-1, AAGCGGCTTGAGGGTAATCAA; sh*Sirt1*-2, AAGCCAGAGATTGTCTTCTTT) and cloned into the pLKO.1-TRC cloning vector, a gift from David Root (Addgene plasmid # 10878) (Moffat et al., 2006). An shRNA targeting *Luciferase* was also designed as a control (sh*Luc*, TGAAACGATATGGGCTGAATA). For lentivirus packaging, foreign DNA (2 μg) was transfected into HEK 293FT cells (1 well of a 6-well-plate) together with the packaging plasmids, *Pax2* (1.5 μg) and *Vsvg* (1 μg), using the Fugene HD transfection reagent (Roche) according to the manufacturer's recommendations. Supernatant containing the lentiviruses was added to mESCs supplied with 8 μg/ml polybrene.

For constitutive overexpression of *Sirt1* or *Sirt1* H355A, a guide RNA (gRNA) targeting a region close to the stop codon of HPRT (*Hprt* gRNA sequence: AAGGGTCCTCCTACGTTGT) and a donor plasmid containing *T2A-Blasticidin-Sirt1*-CAG cassettes flanked by the 5' and 3' homologous arms were co-electroporated into 46C mESCs using the Gene Pulser Xcell System (Bio-Rad) at 320 V, 200 μF in a 0.4-cm cuvettes (Phenix Research Products), and selected with 5 μg/ml blasticidin (InvivoGen) for 5-7 days. The surviving clones were then picked up for genomic DNA PCR analysis. The cDNA of *Sirt1* and *Sirt1* H355A were subcloned from pAd-Track-*Flag-Sirt1* and pAd-Track-*Flag-Sirt1* H355A, gifts of Pere Puigserver (Addgene plasmids # 8438 and #8439) (Rodgers et al., 2005).

For the inducible overexpression system, advanced *rtTA* driven by the CAG promoter was intergraded into the *Rosa26* or *AAVS1* locus via electroporation using engineered zinc-finger nucleases, as described previously (Perez-Pinera et al., 2012). A lentiviral backbone containing tetracycline response element (TRE)-driven *HA-Oct6*, *HA-Otx2*, *HA-Zic2*, *Flag-Sox2, Flag-Pax6, HA-OCT6 K263&268Q, HA-Zfp521 or Flag-Sirt1* was subcloned and used for virus packaging. Medium containing viral particles was then added to the *rtTA* ESCs line for efficient infection.

For *Oct6* knockout, two gRNAs targeting the major open reading frame of *Oct6* were designed (*Oct6* KO gRNA-1, CTTCTGCACTTCGCGGTACG; *Oct6* KO gRNA-2, GCGCGCTAACTGCGCGCCGG) and cloned as previously described (Aparicio-Prat et al., 2015). The

two gRNAs, the CAS9 expression plasmid and a transient blasticidin-resistance gene-expression plasmid were electroporated into *rtTA* mESCs. The cells were selected with 3-10 μg/ml blasticidin for 3 days, and the surviving clones were picked up for genomic DNA PCR analysis. For *Sirt1* knockout in hESCs, two gRNAs targeting the exon1 of *Sirt1* were designed (*Sirt1* KO gRNA-1, CTCCGCGGCCTCTTGCGGAG; *Sirt1* KO gRNA-2, CCGCCGGCACCTCACGCTCT). Cleavage mediated by these dual gRNAs would produce a premature translational termination codon in exon1.

Chromatin Immunoprecipitation (ChIP) Assays

ChIP assays were performed as previously described (Song et al., 2013). Briefly, the day 2.5 mouse neural differentiation derivatives were dissociated into single cells and cross-linked with 1% formaldehyde for 10 min at room temperature, followed by quenching with 0.125 M glycine. Samples were lysed after two washes with PBS and sonicated to generate DNA fragments of approximately 750 bp in length. Then, the chromatin fragments were immunoprecipitated overnight with anti-OCT6 (1:200, Abcam, ab31766) at 4°C. After dissociation from the immunocomplexes, the immunoprecipitated DNAs were quantified by Q-PCR and normalized against the genomic DNA input prepared before immunoprecipitation. The primers used in ChIP-PCR are listed in Table S1.

Immunostaining

For mouse cells, mouse day 4 SFEBs were dissociated into single cells and plated onto 12-mm coverslips coated with 2% (v/v) Matrigel (BD Biosciences) with approximately $(2\pm0.5)\times10^5$ cells for 12~24 hours. For human cells, human neural differentiation derivatives on day 6 were plated into poly-ornithine coated 12-mm coverslips for 3~4 days. Coverslip cultures were then fixed with 4% paraformaldehyde for 10 min at room temperature. After being washed with PBS, the cells were incubated in a penetrating/blocking buffer (10% donkey serum, 0.2% Triton X-100 in PBS) for 1 h at room temperature followed by overnight primary antibody incubation at 4°C. Next, cells were stained with the fluorescently conjugated secondary antibodies (1:2000, Jackson, West Grove, PA) for 1 hour and with Hoechst 33342 (50μg/ml, Sigma, 14533) for 10 min. The following primary antibodies were used: GFP (1:2000, Invitrogen, A6455), N-CADHERIN (1:2000, BD Biosciences, #610920), SOX1 (1:1000, R&D Systems, AF3369), SOX2 (1:1000, R&D Systems, AF2018), PAX6 (1:1000, Covance, PRB-278P), GATA4 (1:500, Santa Cruz, sc-9053), OCT4 (1:1000, Santa Cruz, sc-5279), NANOG (1:1000, Abcam, ab80892) and NESTIN (1:1000, Millipore, MAB5326; 1:1000, Abcam, ab6142).

FACS analysis

To detect the percentage of SOX1-GFP-positive cells, day 3, day 5 or day 7 SFEBs from 46C were dissociated into single cells with trypsin-EDTA, and neutralized with serum. Then the cells were then resuspended in PBS and submitted to FACS analysis, which were performed on a FACSCalibur (BD Biosciences) operating at 488 nm excitation with standard emission filters. A baseline of fluorescence noise was established with undifferentiated mESCs. For the analyses of the cell cycle or apoptosis, SFEBs from 46C were dissociated into single cells with trypsin-EDTA, and neutralized with serum, as specified by the manufacturer (KeyGEN, KGA105 or KGA511).

Immunoprecipitation Assays

Immunoprecipitation assays were performed as described previously (Song et al., 2013). Briefly,

day 2.5 SFEBs were harvested and lysed with lysis buffer (1% Triton X-100 in 50 mM Tris-HCl, pH7.4 containing 150 mM NaCl, 2 mM Na3VO4, 100 mM NaF and protease inhibitors). Cell lysates were incubated overnight with primary antibody or control normal IgG at 4°C. Then, a 5% BSA (w/v, in lysis buffer) coated 1:1 mixture of Ezview Red Protein A Affinity Gel (Sigma, P6486) and Ezview Red Protein G Affinity Gel (Sigma, E3403) was added into the antibody-containing lysates for 1.5 hours. Beads-antibody-protein mixtures were submitted to Western blotting after adequate washing. The following primary antibodies were used for immunoprecipitation: SIRT1 (1:300, Cell Signaling, #8469), OCT6 (1:300, Abcam, ab31766), Ac-Lys (1:300, Upstate, 05-515), mouse normal IgG (1:300, Millipore, 12-371), and rabbit normal IgG (1:300, Millipore, 12-370). To assess the interaction between exogenously expressed proteins, *Flag*-tagged *Sirt1* or *Sirt1* H355A and *HA*-tagged *Oct6* were co-transfected into HEK 293FT cells, and immunoprecipitations were carried out with Ezview Red Anti-FLAG M2 affinity gel (Sigma, F2426) or Ezview Red Anti-HA affinity gel (Sigma, E6779).

Western Blotting

Cells were harvested and lysed with protease inhibitor-containing RIPA buffer. Protein concentrations were standardized using the Pierce BCA Protein Assay Kit (Thermo Scientific). A total of 15 μg of total proteins was separated by SDS-PAGE, transferred to nitrocellulose membranes (NC), and blotted with the following primary antibodies: SIRT1 (1:3000, Millipore, 07-131), OCT6 (1:2000, Abcam, ab31766), Ac-Lys (1:1000, Cell Signaling, #9441), NANOG (1:2000, Abcam, ab80892), Ac-H3K9 (1:2000, Millipore, 06-942), Ac-H4K16 (1:2000, Millipore, 07-329), Histone 3 (1:2000, Millipore, 05-928), Histone 4 (1:1000, Millipore, 05-858), phospho-ERK1/2 (1:2000, Bioworld, AP0484), ERK1/2 (1:2000, Bioworld, BS6426), phospho-GSK3β (Tyr216) (1:2000, Signalway Antibody, #11301), GSK3β (1:2000, Cell Signaling, #9832), GAPDH (1:3000, Sigma, G9545), phospho-SMAD1/5 (1:2000, Cell Signaling, #9511), SMAD1/5/8 (1:1000, Santa Cruz, sc-6031-R), FLAG (1:3000, Sigma, F1804), HA (1:3000, Abcam, ab9110, or 1:2000, Santa Cruz, sc-805 HRP) and β-ACTIN (1:5000, Sigma, A5316).

Fluorometric SIRT1 Activity Assay

To analyze the endogenous SIRT1 deacetylase activity, SIRT1 was immunoprecipitated with anti-SIRT1 (1:300, Millipore, 07-131) from differentiated day 2.5 mouse or day 5 human neural differentiation derivatives with or without environmental stress stimulation, and incubated with NAD^+ (200 μM) and fluorescently labeled acetylated P53 peptide (20 μM), as specified by the manufacturer (Abcam, ab156065). SIRT1 activity was assessed by measuring the fluorescence emission at 440~460 nm following excitation at 350~380 nm.

SUPPLEMENTAL REFERENCES

Aparicio-Prat, E., Arnan, C., Sala, I., Bosch, N., Guigo, R., and Johnson, R. (2015). DECKO: Single-oligo, dual-CRISPR deletion of genomic elements including long non-coding RNAs. BMC Genomics 16, 846.

Moffat, J., Grueneberg, D.A., Yang, X., Kim, S.Y., Kloepfer, A.M., Hinkle, G., Piqani, B., Eisenhaure, T.M., Luo, B., Grenier, J.K., et al. (2006). A lentiviral RNAi library for human and mouse genes applied to an arrayed viral high-content screen. Cell 124, 1283-1298.

Perez-Pinera, P., Ousterout, D.G., Brown, M.T., and Gersbach, C.A. (2012). Gene targeting to the ROSA26 locus directed by engineered zinc finger nucleases. Nucleic acids research 40, 3741-3752.

Rodgers, J.T., Lerin, C., Haas, W., Gygi, S.P., Spiegelman, B.M., and Puigserver, P. (2005). Nutrient control of glucose homeostasis through a complex of PGC-1alpha and SIRT1. Nature 434, 113-118.

Song, C., Zhu, S., Wu, C., and Kang, J. (2013). Histone deacetylase (HDAC) 10 suppresses cervical cancer metastasis through inhibition of matrix metalloproteinase (MMP) 2 and 9 expression. The Journal of biological chemistry 288, 28021-28033.